Effect of synthesis method and morphology on the enhanced CO2 sensing properties of magnesium ferrite MgFe2O4

Thondiyanoor Pisharam Sumangala, Isabelle Pasquet, Lionel Presmanes, Yohann Thimont, Corine Bonningue, Narayanan Venkataramani, Shiva Prasad, Valérie Baco-Carles, Philippe Tailhades, Antoine Barnabé

Effect of synthesis method and morphology on the enhanced CO_2 sensing properties of magnesium ferrite $MgFe_2O_4$

Sumangala T.P.[a], Isabelle Pasquet[a], Lionel Presmanes[a], Yohann Thimont[a], Corine Bonningue[a], N. Venkataramani[b], Shiva Prasad[c,d], Valérie Baco-Carles[a], Philippe Tailhades[a], Antoine Barnabé[a,*]

[a] CIRIMAT, Université de Toulouse, CNRS, Université Toulouse 3 Paul Sabatier, 118 route de Narbonne, 31062 Toulouse Cedex 9, France
[b] Metallurgical Engineering and Materials Science Department, Indian Institute of Technology Bombay, IIT Powai, Mumbai 400076, India
[c] Department of Physics, Indian Institute of Technology Bombay, IIT Powai, Mumbai 400076, India
[d] Institute of Infrastructure Technology Research and Management (IITRAM), Nr. Khokhra Circle, Maninagar (E), Ahmedabad 380026, Gujarat, India

ARTICLE INFO

Keywords:
Ferrite
Oxide
Gas sensor
CO_2

ABSTRACT

The synthesis and characterization of magnesium ferrite $MgFe_2O_4$ prepared by co-precipitation and sol gel combustion is reported. Structural characterization showed that all the samples have single spinel phase. The co-precipitated sample exhibits smaller grains and twice higher BET surface than the sol gel combustion samples. The powder was shaped to dedicated chemo-resistive home-made sensors devices. The electrical properties and sensing properties towards carbon dioxide of both $MgFe_2O_4$ powders were studied. The type of charge carriers were analysed on the basis of the change in resistance in the presence of air and argon. The sensing response towards CO_2 was found to be dependent on the morphology of the powder sample and the CO_2 concentration. A high response of 36% towards 5000 ppm of CO_2 was reached which is good for this gas. The key role of the Mg ions modulating the electrical properties is discussed.

1. Introduction

Carbon dioxide is a greenhouse gas, which affects adversely the health and the environment and hence should be monitored. Carbon dioxide sensing is also interesting as it is useful for proximity sensing for incorporating with the indoor air quality maintenance. This requires the installation of CO_2 sensors in large number. However, the currently available commercial sensors are based on infrared optics and are costly. The use of metal oxide semiconductor (MOS) based sensor would alleviate this issue. But the lower reactivity of CO_2 towards MOS makes it difficult for practical implications.

Recently there have been reports on the use of silicon nanowires for CO_2 sensing [1]. In addition to this, metal oxide and graphene composites have also been found useful for CO_2 sensing [2]. There have been many recent reports on the use of single oxides for CO_2 sensing like copper oxide [3], tin oxide [4], perovskites [5 9], zinc oxide [10,11] and other single phases [12 19]. Composite or functionalized oxides have also been reported as potential candidates for CO_2 sensing [20 26]. Our group has reported using copper oxide copper ferrite composite thin films and powder composites as CO_2 sensors [27 29]. Even if ferrite have been widely studied for many different applications [30 34] including gas sensing [35 40], the use of single spinel ferrite phases for CO_2 detection has rarely been explored before. Among the various ferrites, magnesium ferrite was chosen for studying the CO_2 response. Magnesium ferrite is a magnetic material and finds application in deflection yokes (Mg Zn), microwave devices (Mg Mn), catalysis and biomedical applications and chemical sensing [41 45]. The chemical sensing properties of magnesium ferrite have been studied towards various gases like LPG, ethanol, carbon monoxide, hydrogen sulfide, petrol, chlorine and acetylene [46 51]. However, as compared to the conventional single metal oxide materials, the chemical sensing properties of complex metal oxides towards weakly reactive gases like carbon dioxide is not well explored. Among these mixed oxides, the CO_2 sensing properties of magnesium ferrite have not yet been studied.

In this paper, we report the synthesis of magnesium ferrite by two techniques, co precipitation using oxalate precursor route and sol gel combustion. The effect of synthesis techniques on the structural, morphological, electrical and carbon dioxide sensing properties is reported.

* Corresponding author.
E-mail address: barnabe@chimie.ups-tlse.fr (A. Barnabé).

https://doi.org/10.1016/j.ceramint.2018.07.082

2. Methodology and materials

2.1. Materials and fabrication process

Magnesium ferrite was synthesized by two techniques; co precipitation with oxalate precursor route and sol gel combustion. For co precipitation route magnesium chloride and ferrous chloride were mixed in 1.8:1 ratio (theoretical 1:2 ratio does not yield stoichiometric magnesium ferrite due to the preferential washing away of the Mg ions related to a quite high solubility product of magnesium oxalate compared to iron oxalate) in a mixture of water (60%) and ethylene glycol (40%) to form a 2 M solution. Hydrochloric acid (1%) was added to prevent the oxidation of metal salts. The mixture was stirred using a magnetic stirrer. In order to precipitate metal ions, this solution was added to the solution of oxalic acid (10% extra to the total metal ion content) with 0.5 M ethanol using a peristaltic pump. The entire mixture was stirred mechanically for 30 min. The resultant suspension was washed by centrifuging (3500 rpm, 10 min) followed by mechanical stirring (30 min) for 3 times using de ionized water. This was followed by a washing with ethanol. The obtained oxalate precursor was dried at 80 °C in oven for 8 h. The oxalate was then decomposed in air at 350 °C at a heating rate of 50 °C/h and was then calcined at 600 °C for 1 h. This powder was further calcined at 800 °C for 1 h for having the same calcinations temperature as that of the sol gel combusted sample.

For sol gel combustion, metal nitrates of magnesium and iron was taken in 1:2 ratio and dissolved in de ionized water using a magnetic stirrer equipped with a hot plate at 60 °C. Citric acid was added to this solution in 1:1 ratio of the total metal ion content. The pH of solution was brought to 7 by adding ammonium hydroxide. The mixture turned in to a thick solution, a transparent gel and then to a thick gel with time. At this point the temperature of the hot plate was increased to 80 °C. This initiated the combustion which continued until all the citric acid has been burned. A fluffy powder was obtained after the combustion which was then ball milled using yttrium stabilized zirconia balls for 24 h. The powder was then calcined at 800 °C to obtain pure phase of magnesium ferrite.

The phase of the synthesized powder was checked using X Ray Diffraction (XRD) using a D4 Endeavor Bruker diffractometer equipped with a copper anode and LynxEye 2D detector. The lattice parameter of the phase was calculated from Rietveld refinement using Fullprof software. The surface area of the particles was measured using BET single point Micromeritics Automate 23 surface area analyser. The morphology of both the powders was studied by JEOL JSM 6400 Scanning Electron Microscope (SEM). The powder was fabricated to a device on alumina substrate without any change of the microstructure of the sample. The elaboration of powder in the form device requires achieving a proper contact between the active material and the electrode. This was done by the use of silver oxalate as the precursor for contact. A paste made with the magnesium ferrite powders and ethylene glycol was coated on the substrate with electrode. This was again kept in vacuum for 24 h and was then heated to 780 °C for 1 h with a heating rate of 150 °C/hour and was allowed to cool normally in the furnace. The detailed procedure is mentioned elsewhere [29].

2.2. Experimental set up

The CO_2 sensing properties of the device were studied using a chemical sensor set up. The schematic of this set up is given in Fig. 1.

The sensing was performed using a Linkam cell attached with a thermal controller. The CO_2 sensing was measured by alternately passing dry air and 5000 ppm CO_2 in dry air. The flow rate of both the gases was controlled using separate Brooks 5800S mass flow controllers (MFC). The flow rate and duration of gas through these mass flow controllers were further controlled using a pneumatic valve (PV) which in turn was controlled using an electro valve (EV). The incorporation of two mass flow controllers made it possible to change the concentration of the test gas from 5000 ppm to 1000 ppm. A ball valve (BV) was added to the line to prevent a back streaming of the gas. The resistance in the presence of air and CO_2 was measured using Keithley 2400 source meter. The set up consisted of a computer which was connected to the temperature controller of the Linkam cell, the mass flow controllers, electro valve and the Keithley source meter. The interfacing and controlling was executed using LabVIEW software. The response towards CO_2 was calculated using Eq. (1)

$$R(\%)=\frac{R_{Air}-R_{CO2}}{R_{Air}} x\ 100 \quad (1)$$

3. Results and discussion

3.1. Structural characterization

Fig. 2 gives the XRD patterns of magnesium ferrite prepared by co precipitation and sol gel combustion methods. All the peaks could be indexed with magnesium ferrite spinel phase. This indicates that both the powders corresponds to single phase magnesium ferrite (space group F $d\bar{3}m$). The lattice parameter of both samples was calculated by performing Rietveld refinement implemented in the Fullprof program. The obtained lattice parameters were 8.385 (1) Å and 8.383 (2) Å for the co precipitated and combusted powder respectively. It could be noted that the lattice parameters of both samples are nearly the same. It is therefore not possible to make differences related to a small change in magnesium content and/or cationic distribution on these samples. Magnesium ferrite is normally 90% inverse ferrite in bulk form and the lattice parameter of bulk material is 8.36 Å [52]. The lattice parameter obtained on the synthesized magnesium ferrite powder samples is higher than the bulk and indicates that the inversion factor is lower than 0.9. A calculation of inversion factor based on Poix's method [53,54] indicates that it is in between 0.7 and 0.75 for the samples. In this method, lattice constants were calculated using cation oxygen distances listed in Table 1 deduced from the effective ionic radii according to R.D. Shannon [55].

The lattice constant of a spinel oxide $M[M'_2]O_4$ is then defined by Eq. (2):

$$a = 2.0995\ A + [5.8182\ B^2 - 1.4107\ A^2]^{1/2} \quad (2)$$

where $A = \Sigma\ n_i\ (M_i\ O)_{Td}$ and $B = 0.5\ \Sigma\ n_j\ (M'_j\ O)_{Oh}$ represents the cation to oxygen average distances in tetrahedral and octahedral sub lattices respectively. In this calculation, n_i and n_j are the respective quantities of M and M′ cations per formula unit, and $(Mi\ O)_{Td}$ and $(M'i\ O)_{Oh}$ are the cation oxygen distances in tetrahedral and octahedral sites. Thus the XRD patterns confirm that the samples have the same structure irrespective of the synthesis technique adopted.

3.2. Microstructural analysis

The XRD patterns in Fig. 2, indicated the similarity in the structure of both samples. However, it could be observed from Fig. 2 that the peak broadening is not the same in case of both samples. The peaks of co precipitated powder are broader than that of the combusted powder. This indicates that there is a difference in the crystallite size between the two samples. The crystallite size of both samples was calculated following the Williamson and Hall method approach. The obtained crystallite sizes were 22 nm and 126 nm for the co precipitated and combusted samples respectively. This shows that the combusted samples consist of crystallites which are nearly 5 times bigger than the co precipitated sample.

To confirm the difference in the microstructure, the samples were observed by SEM. Fig. 3(a) and Fig. 3(b) gives the SEM images of both the magnesium ferrite powders. At lower magnification, Fig. 3(c) and Fig. 3(d) show SEM images of both powders coated onto the porous silver electrode.

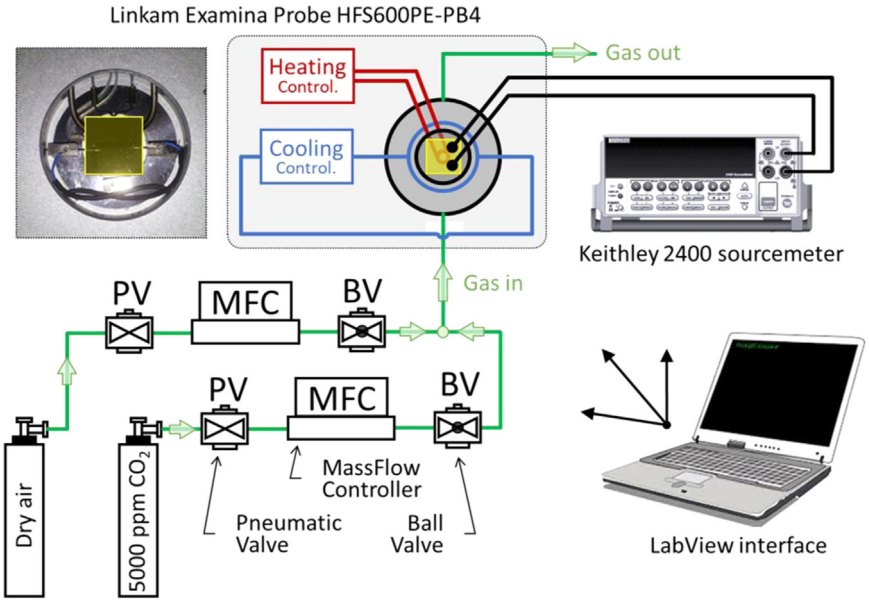

Fig. 1. Schematic of the CO_2 sensing set up.

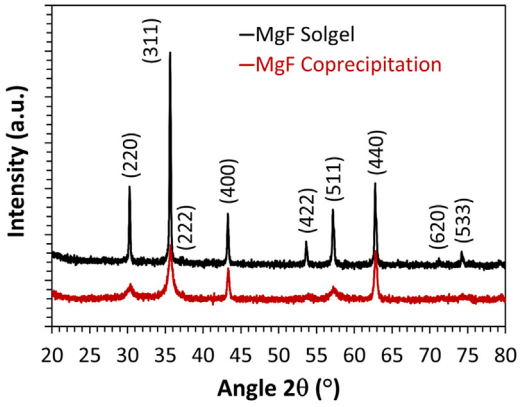

Fig. 2. X-ray diffraction of magnesium ferrite synthesized by co-precipitation and sol gel combustion routes.

Table 1
Cation – oxygen distance according to R.D. Shannon effective ionic radii [55].

Cation	$(M_i\text{-}O)_{Td}$ (Å)	$(M'_j\text{-}O)_{Oh}$ (Å)
Fe^{2+}	2.003	2.154
Fe^{3+}	1.855	2.020
Mg^{2+}	1.990	2.106

From Fig. 3, it is observed that the morphology of both powders is different. Magnesium ferrite synthesized by co precipitation method has elongated particles and forms a porous assembly. The average length of these particles was 0.9 ± 0.2 μm and breadth 0.18 ± 0.06 μm. This indicates that each particle contain many crys tallites. The width of a single particle is greater than that the crystallite size and this shows that the elongated particles are formed by in dividual crystallites which are arranged along their length and breadth to form a needle like structure. Magnesium ferrite by sol gel combustion has spherical particles which are bound to each other to form hard clusters. The average particle size estimated from the SEM image is 0.21 ± 0.07 μm. This shows that the particles consist of either one or two crystallites.

The SEM observation yields that the samples with the same com position results in different microstructure. This is important for the application of these materials in gas sensing because sensing capability depends of the specific surface. This is due to the fact that the chemical sensing is dependent on the number of active sites available for che mical reaction. Thus, to quantify the available surface sites, a BET surface area analysis was performed on both the samples. The surface area obtained was 16.2 and 9.0 m^2/g, for the co precipitated and combusted powder respectively. This shows that the surface area of the co precipitated powder is nearly twice of the combusted one. The particle size of the combusted powder evaluated from SEM is smaller than the co precipitated one. This means the surface area of the com busted powder should be higher. But, this case would be applicable only if both the samples have the same morphology and microstructure. The higher surface area of the co precipitated particle could be due to the needle like morphology and a high porosity resulting from the de composition process of the starting oxalate, which in the end yields more surface area than corresponding spherical particle with the same dimension. In addition to this, the lower surface area of the combusted particles could also be assigned to the presence of agglomerates which considerably reduces the available active surface.

3.3. Electrical properties

In the mechanism proposed by Verwey, electrical conduction occurs by charge hopping between transition metal cations from the same element, with different oxidation state, and located in the same sub lattice [56]. $MgFe_2O_4$ is a n type semiconductor [46] and the conduc tion is then due to electron hopping mechanism: $Fe^{3+} + e \leftrightarrow Fe^{2+}$ in octahedral site. The temperature dependence of the conductivity in ferrites at a high temperature can be expressed as:

$$\frac{1}{R}=\frac{A}{T}e^{-\frac{E_a}{k_BT}} \quad (3)$$

where R is the electrical resistance, A a constant, T the absolute tem perature, E_a the hopping activation energy and k_B the Boltzmann's constant.

The electrical properties of the sample were studied by heating the sample in the 100 300 °C range. Arrhenius plots (ln T/R versus $1/k_BT$) given in Fig. 4 are almost linear which confirm the hopping type con duction. We can also observe that the resistance values of both samples are quite closed. The slight difference observed between the two de vices may be the consequence, on the one hand, of the coarser

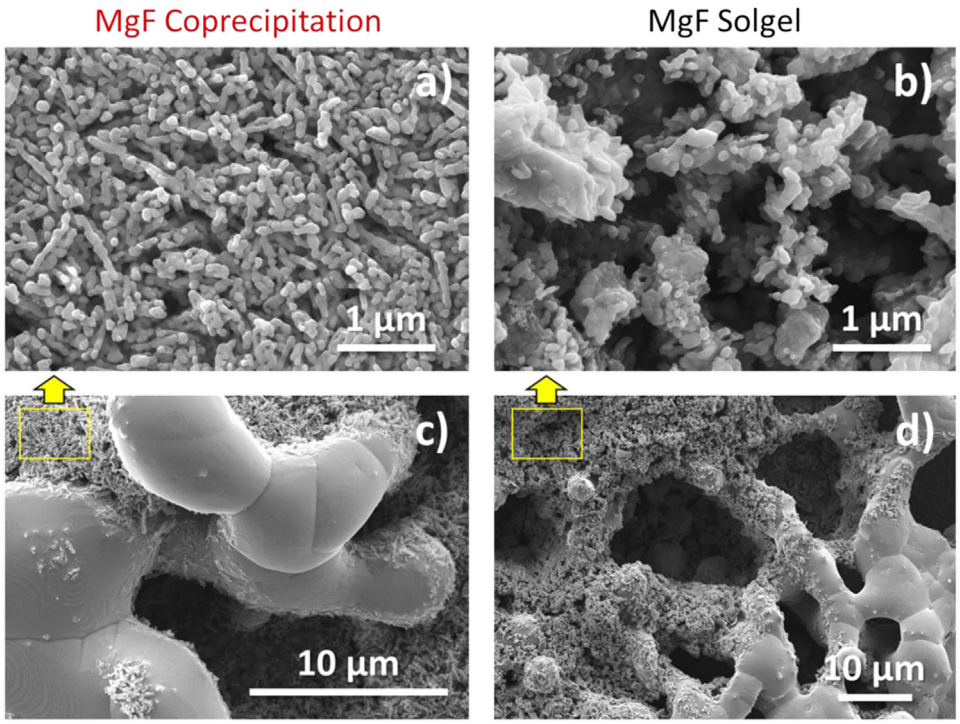

Fig. 3. SEM micrograph of magnesium ferrite powders prepared by co-precipitation [a), c)] and sol gel combustion [b), d)] coated on porous silver electrode for electrical and gas sensing measurements.

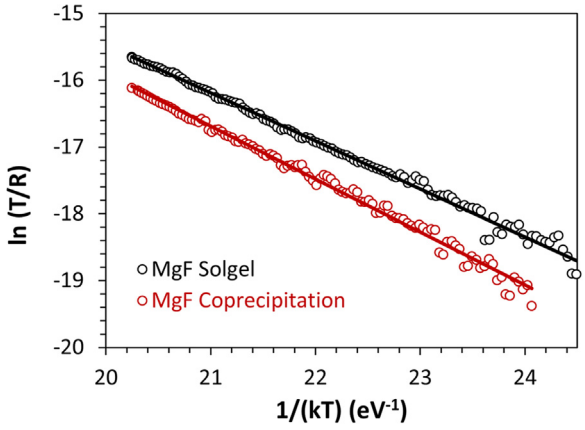

Fig. 4. Arrhenius plot of magnesium ferrite co-precipitated and combusted sample.

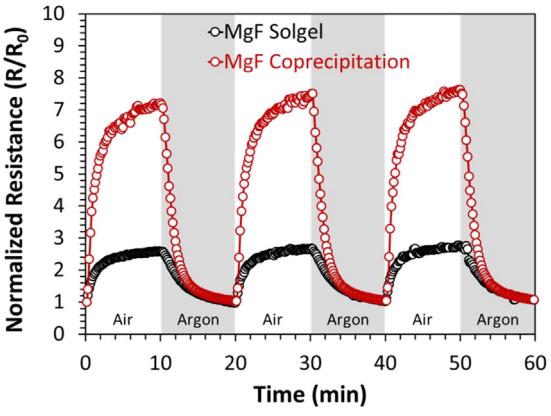

Fig. 5. Variation of the response R/R_0 at 300 °C of magnesium ferrite samples co-precipitated and sol-gel combusted in the presence of air and argon.

microstructure of the ferrite obtained by combustion, and on the other hand, of the variation of the geometrical characteristics (distance be tween the electrodes and the thickness of the sensitive layers) which is due to the method of preparation used. The slope of the plot gives the hopping activation energy (E_a) and was calculated to be 0.79 and 0.72 eV for co precipitated and sol gel combusted samples respectively. This shows that the activation energy is in the same range for the both preparation.

Using the resistance variation during Air Ar alternations it is pos sible to define if the material has a p type or n type semiconducting behavior.

The change in resistance (R/R_0) of both magnesium ferrite samples was studied under air and argon alternations (Fig. 5). This experiment, gives an idea about the charge carrier present in the sample. When an n type semiconducting oxide is put in contact with air, the adsorption of oxygen species (mainly O_2 and O) occurs at the surface, which in turn mobilizes electrons, causing depletion in number of carriers at its surface and thus leading to an increase of the electrical resistance. In the case of p type oxide, it is the opposite phenomenon, which occurs and the mobilization of electrons causes an increase in the hole con centration at the surface and thus lead to a decrease in the resistance. When the oxide samples are brought under argon, the desorption of oxygen species releases the initially trapped electrons which lead to a recovery of the electrical properties by a decrease in the resistance for the case of a n type or conversely an increase in the case of a p type. It is clear from Fig. 5 that the resistance of magnesium ferrite increases in air while it decreases with the insertion of argon. That demonstrates the n type behavior of both magnesium ferrite samples. We can notice that the ratio R/R_0 is much higher in the case of co precipitated sample, which can be due to the higher specific surface area of the ferrite particles prepared by this route.

3.4. Carbon dioxide sensing

CO_2 sensing tests carried out with both magnesium ferrite samples

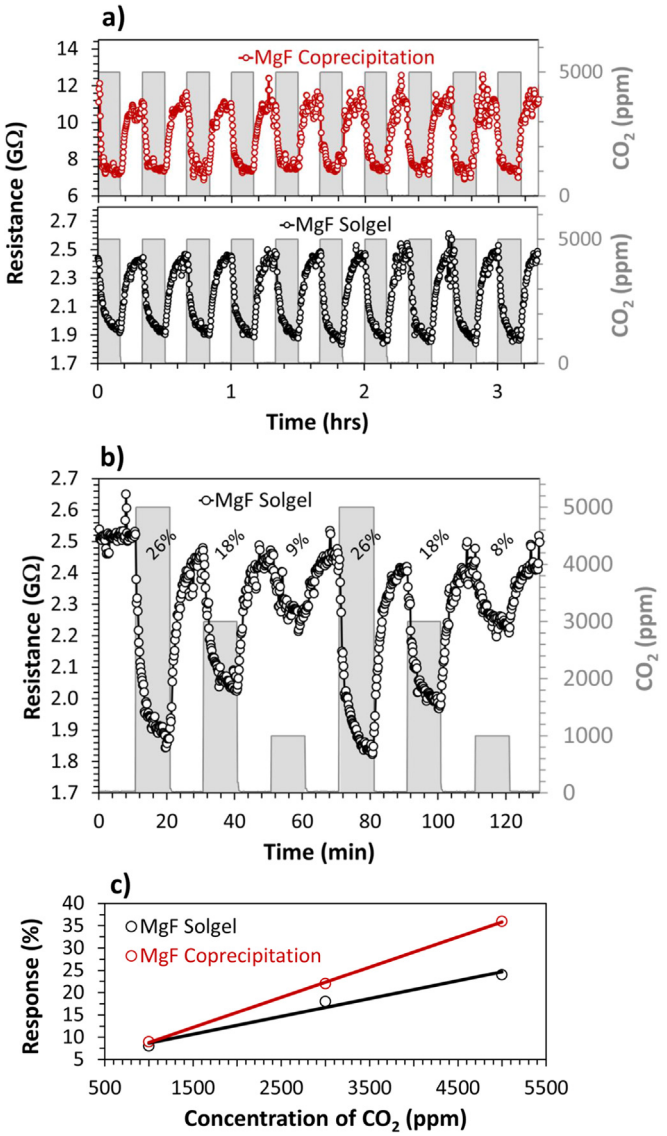

Fig. 6. (a) Change in resistance at 300 °C of co-precipitated and sol gel combusted magnesium ferrite samples in the presence of 5000 ppm CO_2. (b) Variation of the resistance at 300 °C with concentration for Mg ferrite sol-gel combusted sample. (c) Variation of the resistance at 300 °C as a function of the CO2 concentration for both samples.

Table 2
Response, response time and recovery time towards 5000 ppm CO_2 of magnesium ferrite samples prepared by both routes.

Sample	Response (%)	Response time (min)	Recovery time (min)
MgF Co-precipitation	36 ± 2	2	4
MgF Sol-gel combustion	24 ± 2	5	5

are reported in Fig. 6. In Fig. 6(a), we can observe that the resistance decreases with the insertion of 5000 ppm of CO_2 for both samples. The experiments performed with a step size of 10 min indicate that this time is sufficient for the co precipitated sample to saturate. However, the combusted sample has not reached saturation in the same time interval as the co precipitated sample. Fig. 6(a) shows the repeatability over 10 cycles with co precipitated and sol gel combusted samples. The signal remains almost the same over multiple cycles in both test devices which is in agreement with a complete reversibility of the CO_2 mechanism adsorption. The noisy data in case of co precipitated sample can be attributed to the higher resistance (up to 11 GΩ) in comparison with the combusted powder (2.5 GΩ) which leads to instrumental limit. This result demonstrates the sensitivity of both samples towards 5000 ppm of CO_2. The response and the response transients (response time and recovery time) towards 5000 ppm of CO_2 are given in Table 2.

It can be observed from Table 2, that magnesium ferrite samples prepared by both techniques are sensitive to CO_2. However, the re sponse of magnesium ferrite obtained by co precipitation is higher than that with sol gel combustion. In addition to this, the magnesium ferrite co precipitated sample has faster transient response (faster response and recovery time) in comparison with the sol gel combusted one. The change in the response of both magnesium ferrite samples towards CO_2 could be attributed to the different microstructure. The co precipitated sample had more surface area and elongated particles which would have led to more chemically reactive surface sites.

The CO_2 sensing response of devices made with both magnesium ferrite powders was also studied by varying the concentration to 5000, 3000 and 1000 ppm. The change in response with CO_2 concentration for magnesium ferrite sol gel combusted sample is shown in Fig. 6(b). The response obtained at each concentration for both samples is com pared in Fig. 6(c). The response of both samples increase linearly with the concentration of CO_2. This result confirms that the response is de pendent on the concentration of CO_2.

The dynamic responses of both co precipitated and sol gel magne sium ferrite samples towards 5000 ppm of CO_2 (R = 36% and R = 24% respectively) are highly increased in comparison with those of co pre cipitated copper ferrite (CuF) samples (R = 10%) measured in the same experimental conditions [33]. Chemoresistive CO_2 sensing perfor mances of other various oxide based materials [57 59] are reported in Table 3 for similar experimental conditions, i.e. for 4000 5000 ppm of CO_2 in dry air and various operating temperatures. We can notice from this data that the dynamic response of 36% obtained with the co pre cipitated magnesium ferrite powder sample is of the same order of magnitude as SnO_2 based and/or ZnO based doped nanostructured materials. In our previous study [33], CuF samples showed typical n type gas sensing properties with 1) a decrease in the resistance upon Ar exposure and 2) an increase of the resistance upon CO_2 exposure into the air. The increase in resistance value when n type sample is exposed to a CO_2 pulse can be explained by the reaction of adsorbed oxygen ions with the CO_2 gas leading to the extraction of electrons from the con duction band [11]. The most probable assumption is that sensing me chanism of $MgFe_2O_4$ layer could be controlled by the work function variations due to adsorption of carbonate at the surface of the grains. In our case, the use of dry air in our experiment can lead to the formation of iron and/or magnesium carbonates activated both by oxygen and carbon dioxide.

In this work, n type MgF samples showed identical behavior than CuF ferrite upon Ar exposure but the resistance of the samples de creased when CO_2 gas is introduced. This unexpected result suggests that, in presence of Mg, the operating sensing mechanism is likely to be different from that observed for copper ferrite. This result was pre viously observed on others n type semiconducting active materials as for instance LaOCl ZnO [23], SnO_2 [60]. When comparing ZnO and Ca doped ZnO materials, R. Dhahri et al. [10] observed similar behavior, i.e. an opposite direction of resistance changes with the Ca doping. They highlighted the key role of Ca addition on the ZnO surface in the sensing mechanism: Ca acts as basic center and therefore is able to absorb more strongly the acid CO_2 gas molecules compared to a pristine ZnO surface. Through the formation of adsorbed carbonates and bi carbonates, electrons are releasing and consequently strongly decrease the resistance. Similarly, our results suggest that, in ferrite surface, Mg ions plays a similar key role in the CO_2 adsorption and enhance the CO_3 or HCO_3 or any complex ligands formation rather than change in depletion region (Debye layer) which strongly impact the carrier transport in particular at grain boundary. Thus the direction of the

Table 3
Comparative chemoresistive CO_2 sensing performances of various oxide-based materials reported in the literature as well as the magnesium ferrite of the present study.

Material	Response $(R_{CO2}-R_{air})/R_{air}$ (%)	Operating conditions	Ref.
$BaTiO_3$-CuO-$LaCl_3$	+ 2.4	5000 ppm CO_2 at 550 °C in dry air	[57]
LaOCl	+ 300	5000 ppm CO_2 at 260 °C in dry air	[58]
$BaTiO_3$-CuO	+ 4	5000 ppm CO_2 at 300 °C in dry air	[25]
$Ca_{10}(PO_4)_6(OH)_2$	+ 200	5000 ppm CO_2 at 165 °C in dry air	[16]
CdO	20	5000 ppm CO_2 at 250 °C in dry air	[18]
SnO_2-LaOCl	85	4000 ppm CO_2 at 250 °C in dry air	[21]
$La_{0.8}Sr_{0.2}FeO_3$	+ 36	4000 ppm CO_2 at 380 °C in dry air	[6]
ZnO-LaOCl	75	4000 ppm CO_2 at 400 °C in dry air	[22]
Sm_2O_3	6	4000 ppm CO_2 at 400 °C in dry air	[14]
$CuFe_2O_4$-CuO	40	5000 ppm CO_2 at 250 °C in dry air	[28]
ZnO:Ca 5%^{at}	30	5000 ppm CO_2 at 450 °C in dry air	[10]
SnO_2	8	5000 ppm CO_2 at 240 °C in dry air	[4]
ZnO:La 50%^{at}	+ 65	5000 ppm CO_2 at 400 °C in dry air	[20]
SnO_2-$LaFeO_3$	+ 170	4000 ppm CO_2 at 250 °C in dry air	[24]
Co_3O_4	+ 20	5000 ppm CO_2 at 150 °C in dry air	[59]
SnO_2-LaOCl	76	5000 ppm CO_2 at 300 °C in dry air	[23]
$CuFe_2O_4$	+ 10	5000 ppm CO_2 at 450 °C in dry air	[29]
$MgFe_2O_4$	+ 36	5000 ppm CO_2 at 450 °C in dry air	This work

change in resistance is opposite.

4. Conclusion

In summary, magnesium ferrite nanoparticles were synthesized by two chemical routes; co precipitation with oxalate precursor and sol gel combustion. Both these samples had similar composition and lattice parameter. However, the microstructure of both samples was different. The BET surface area of co precipitated sample was greater (nearly twice) than that of sol gel combusted sample and consisted of elongated grains. The Air Ar measurement performed on both samples showed that the samples contained n type charge carriers. Both these samples showed significant response towards CO_2. The sensing response of co precipitated sample was greater (36%) than the sol gel combusted sample (24%). The response of the sample was dependent on the powder morphology and the sample microstructure, which were in turn dependent on the synthesis technique used. An opposite direction of resistance change was observed for the Mg ferrite in comparison with Cu ferrite or other conventional n type semiconducting materials. This suggests that, as in the case of Ca in zincite material, Mg generates different reaction mechanisms with gas in spinel ferrite. These results show that $MgFe_2O_4$ material is a good candidate for low cost CO_2 sensing device.

Acknowledgments

This work was supported by the ANR France [grant number 13 IS08 0002 01] and DST India [grant number 14IFCPAR001] MonaSens project.

References

[1] S. Naama, T. Hadjersi, A. Keffous, G. Nezzal, CO_2 gas sensor based on silicon nanowires modified with metal nanoparticles, Mater. Sci. Semicond. Process. 38 (2015) 367–372.
[2] S. Lee, J. Oh, D. Kim, Y. Piao, A sensitive electrochemical sensor using an iron oxide/graphene composite for the simultaneous detection of heavy metal ions, Talanta 160 (2016) 528–536.
[3] N.B. Tanvir, C. Wilbertz, S. Steinhauer, A. Köck, G. Urban, O. Yurchenko, Work function based CO_2 gas sensing using metal oxide nanoparticles at room temperature, Mater. Today.: Proc. 2 (2015) 4190–4195.
[4] D. Wang, Y. Chen, Z. Liu, L. Li, C. Shi, H. Qin, CO_2-sensing properties and mechanism of nano-SnO_2 thick-film sensor, Sens. Actuators B: Chem. 227 (2016) 73–84.
[5] S. Mulmi, R. Kannan, V. Thangadurai, CO_2 and SO_2 tolerant Fe-doped metal oxides for solid state gas sensors, Solid State Ion. 262 (2014) 274–278.
[6] K. Fan, H. Qin, L. Wang, L. Ju, J. Hu, CO_2 gas sensors based on $La_{1-x}Sr_xFeO_3$ nanocrystalline powders, Sens. Actuators B: Chem. 177 (2013) 265–269.
[7] L. Gómez, V. Galeano, R. Parra, C.R. Michel, C. Paucar, O. Morán, Carbon dioxide gas sensing properties of ordered oxygen deficient perovskite $LnBaCo_2O_{5+\delta}$ (Ln = La, Eu), Sens. Actuators B: Chem. 221 (2015) 1455–1460.
[8] H. Jaouali, N. Hamrouni, M.F. Moussa, M.A. Nsib, A. Centeno, G. Neri Bonavita, S.G. Leonardi, $LaFeO_3$ ceramics as selective oxygen sensors at mild temperature, Ceram. Int. 44 (2018) 4183–4189.
[9] L. Gildo-Ortiz, J. Reyes-Gómez, J.M. Flores-Álvarez, H. Guillén-Bonilla, M. de la, L. Olvera, V.M.R. Betancourtt, Y. Verde-Gómez, A. Guillén-Cervantes, J. Santoyo-Salazar, Synthesis, characterization and sensitivity tests of perovskite-type $LaFeO_3$ nanoparticles in CO and propane atmospheres, Ceram. Int. 42 (2016) 18821–18827.
[10] R. Dhahri, M. Hjiri, L. El Mir, E. Fazio, F. Neri, F. Barreca, N. Donato, A. Bonavita, S.G. Leonardi, G. Neri, ZnO:Ca nanopowders with enhanced CO_2 sensing properties, J. Phys. D 48 (2015) 255503.
[11] P.K. Kannan, R. Saraswathi, J.B.B. Rayappan, CO_2 gas sensing properties of DC reactive magnetron sputtered ZnO thin film, Ceram. Int. 40 (2014) 13115–13122.
[12] L. Li, H. Qin, C. Shi, L. Zhang, Y. Chen, J. Hu, CO_2 sensing properties of $La_{1-x}Ba_xFeO_3$ thick film and packed powder sensors, RSC Adv. 5 (2015) 103073–103081.
[13] D. Mardare, N. Cornei, C. Mita, D. Florea, A. Stancu, V. Tiron, A. Manole, C. Adomnitei, Low temperature TiO_2 based gas sensors for CO_2, Ceram. Int. 42 (2016) 7353–7359.
[14] C.R. Michel, A.H. Martínez-Preciado, R. Parra, C.M. Aldao, M.A. Ponce, Novel CO_2 and CO gas sensor based on nanostructured Sm_2O_3 hollow microspheres, Sens. Actuators B: Chem. 202 (2014) 1220–1228.
[15] J.P. Morán-Lázaro, O. Blanco, V.M. Rodríguez-Betancourtt, J. Reyes-Gómez, C.R. Michel, Enhanced CO_2-sensing response of nanostructured cobalt aluminate synthesized using a microwave-assisted colloidal method, Sens. Actuators B: Chem. 226 (2016) 518–524.
[16] R.U. Mene, M.P. Mahabole, R.S. Khairnar, Surface modified hydroxyapatite thick films for CO_2 gas sensing application: effect of swift heavy ion irradiation, Radiat. Phys. Chem. 80 (2011) 682–687.
[17] A.A. Yadav, A.C. Lokhande, R.B. Pujari, J.H. Kim, C.D. Lokhande, The synthesis of multifunctional porous honey comb-like La_2O_3 thin film for supercapacitor and gas sensor applications, J. Colloid Interface Sci. 484 (2016) 51–59.
[18] T. Krishnakumar, R. Jayaprakash, T. Prakash, D. Sathyaraj, N. Donato, S. Licoccia, M. Latino, A. Stassi, G. Neri, CdO-based nanostructures as novel CO_2 gas sensors, Nanotechnology 22 (2011) 325501.
[19] S. Sen, P. Anand, M. Narjinary, S.K. Md. Mursalin, R. Manna, Ethanol sensing evaluation of sol–gel barium calcium ferrite, Ceram. Int. 42 (2016) 12581–12585.
[20] Y.-J. Jeong, C. Balamurugan, D.-W. Lee, Enhanced CO_2 gas-sensing performance of ZnO nanopowder by La loaded during simple hydrothermal method, Sens. Actuators B: Chem. 229 (2016) 288–296.
[21] D.D. Trung, L.D. Toan, H.S. Hong, T.D. Lam, T. Trung, N.V. Hieu, Selective detection of carbon dioxide using LaOCl-functionalized SnO_2 nanowires for air-quality monitoring, Talanta 88 (2012) 152–159.
[22] N.V. Hieu, N.D. Khoang, D.D. Trung, L.D. Toan, N.V. Duy, N.D. Hoa, Comparative study on CO_2 and CO sensing performance of LaOCl-coated ZnO nanowires, J. Hazard. Mater. 244–245 (2013) 209–216.
[23] Y. Xiong, Q. Xue, C. Ling, W. Lu, D. Ding, L. Zhu, X. Li, Effective CO_2 detection based on LaOCl-doped SnO_2 nanofibers: insight into the role of oxygen in carrier gas, Sens. Actuators B: Chem. 241 (2017) 725–734.
[24] W. Zhang, C. Xie, G. Zhang, J. Zhang, S. Zhang, D. Zeng, Porous $LaFeO_3$/SnO_2 nanocomposite film for CO_2 detection with high sensitivity, Mater. Chem. Phys. 186 (2017) 228–236.
[25] G.G. Mandayo, J. Herrán, I. Castro-Hurtado, E. Castaño, Performance of a CO_2 impedimetric sensor prototype for air quality monitoring, Sensors 11 (2011) 5047–5057.

[26] J. Herrán, O. Fernández-González, I. Castro-Hurtado, T. Romero, G.G. Mandayo, E. Castaño, Photoactivated solid-state gas sensor for carbon dioxide detection at room temperature, Sens. Actuators B: Chem. 149 (2010) 368–372.

[27] F. Chapelle, L. Oudrhiri-Hassani, A. Presmanes, P. Barnabé, Tailhades, CO_2 sensing properties of semiconducting copper oxide and spinel ferrite nanocomposite thin films, Appl. Surf. Sci. 256 (2010) 4715–4719.

[28] I. Chapelle, S. El Younsi, Y. Vitale, T. Thimont, L. Nelis, A. Presmanes, P. Barnabé, Tailhades, Improved semiconducting $CuO/CuFe_2O_4$ nanostructured thin films for CO_2 gas sensing, Sens. Actuators B: Chem. 204 (2014) 407–413.

[29] T.P. Sumangala, Y. Thimont, V.B. Carles, L. Presmanes, C. Bonningue, I. Pasquet, P. Tailhades, A. Barnabé, Study on the effect of cuprite content on the electrical and CO_2 sensing properties of cuprite-copper ferrite nanopowder composites, J. Alloy. Compd. 695 (2017) 937–943.

[30] J. Mürbe, J. Töpfer, Ni-Cu-Zn ferrites for low temperature firing: i. ferrite composition and its effect on sintering behavior and permeability, J. Electroceram. 15 (2005) 215–221.

[31] P. Tailhades, L. Presmanes, I. Pasquet, C. Bonningue, F. Laporte, Spinel oxides thin films for write-once optical recording with blue laser sources, Trans. Magn. Soc. Jpn. 2 (2002) 198–201.

[32] S. Roy, S.B. Majumder, Recent advances in multiferroic thin films and composites, J. Alloy. Compd. 538 (2012) 153.

[33] H.F. Wang, R. Kavanagh, Y.L. Guo, Y. Guo, G. Lu, P. Hu, Origin of extraordinarily high catalytic activity of Co3O4 and its morphological chemistry for CO oxidation at low temperature, J. Catal. 296 (2012) 110.

[34] Z. Šimša, P. Thailhades, L. Presmanes, C. Bonningue, Magneto-optical properties of manganese ferrite films, J. Magn. Magn. Mater. 242–245 (2002) 381–383.

[35] C.V.G. Reddy, S.V. Manorama, V.J.J. Rao, Preparation and characterization of ferrites as gas sensor materials, J. Mater. Sci. Lett. 19 (2000) 775–778.

[36] K.A. Gross Sutkaa, Spinel ferrite oxide semiconductor gas sensors, Sens. Actuators B: Chem. 222 (2016) 95–105.

[37] S. Ghosh, U. Chowdhury, S. Roy, R. Bandyopadhyay, Detection of low ppm carbon monoxide with charge ordered $LuFe_2O_4$ gas sensor – a novel sensing mechanism, Ceram. Int. 42 (2016) 14944–14948.

[38] W. Zhao, H. Lan, J. Gong, R. Bai, S. Ramachandran, F. Liu, Wang, Highly sensitive acetone-sensing properties of Pt-decorated $CuFe_2O_4$ nanotubes prepared by electrospinning, Ceram. Int. 44 (2018) 2856–2863.

[39] R. Wu, C.W. Lin, W.J. Tseng, Preparation of electrospun Cu-doped α-Fe_2O_3 semiconductor nanofibers for NO_2 gas sensor, Ceram. Int. 43 (2017) S535–S540.

[40] F. Falsahi, B. Hashemi, A. Mirzaei, E. Fazio, F. Neri, N. Donato, S.G. Leonardi, G. Neri, Sm-doped cobalt ferrite nanoparticles: a novel sensing material for conductometric hydrogen leak sensor, Ceram. Int. 43 (2017) 1029–1037.

[41] M. Sugimoto, The past, present, and future of ferrites, J. Am. Ceram. Soc. 82 (1999) 269–280.

[42] T. Maehera, K. Konishi, T. Kamimori, H. Aono, T. Naohara, H. Kikkawa, Y. Watanabe, K. Kawachi, Heating of ferrite powder by an AC magnetic field for local hyperthermia, Jpn. J. Appl. Phys. 41 (2002) 1620–1621.

[43] G. Busca, E. Finocchio, V. Lorenzelli, M. Trombetta, S.A. Rossini, IR study of alkene allylic activation on magnesium ferrite and alumina catalysts, J. Chem. Soc. Faraday Trans. 92 (1996) 4687–4693.

[44] T.P. Sumangala, C. Mahender, N. Venkataramani, S. Prasad, A study of nanosized magnesium ferrite particles with high magnetic moment, J. Magn. Magn. Mater. 382 (2015) 225–232.

[45] T.P. Sumangala, C. Mahender, B.N. Sahu, N. Venkataramani, S. Prasad, Study of magnesium ferrite nano particles with excess iron content, Physica B 448 (2014) 312–315.

[46] Y.L. Liu, Z.M. Liu, Y. Yang, H.F. Yang, G.L. Shen, R.Q. Yu, Simple synthesis of $MgFe_2O_4$ nanoparticles as gas sensing materials, Sens. Actuators B: Chem. 107 (2005) 600–604.

[47] N.S. Chen, X.J. Yang, E.S. Liu, J.L. Huang, Reducing gas-sensing properties of ferrite compounds MFe_2O_4 (M = Cu, Zn, Cd and Mg), Sens. Actuators B: Chem. 66 (2000) 178–180.

[48] D.C. Bharti, K. Mukherjee, S.B. Majumder, Wet chemical synthesis and gas sensing properties of magnesium zinc ferrite nano-particles, Mater. Chem. Phys. 120 (2010) 509–517.

[49] E. Doroftei, N. Rezlescu, P.D. Rezlescu, Popa, Magnesium ferrite with Sn^{4+} and / or Mo^{6+} substitutions as sensing element for acetone and ethanol, Rom. J. Phys. 51 (2006) 631–640.

[50] S. Darshane, I.S. Mulla, Influence of palladium on gas-sensing performance of magnesium ferrite nanoparticles, Mater. Chem. Phys. 119 (2010) 319–323.

[51] B. Gadkari, T.J. Shinde, P.N. Vasambekar, Effect of Sm^{3+} ion addition on gas sensing properties of $Mg_{1-x}Cd_xFe_2O$ system, Sens. Actuators B: Chem. 178 (2013) 34–39.

[52] J. Smit, H.P.J. Wijn, Ferrites : physical properties of ferrimagnetic oxides in relation to their technical applications, N.V. Philips, Eindhoven, 1959.

[53] P. Poix, Liaison interatomique et propriétés des composés minéraux, Seides, Paris, 1968, p. 82,

[54] P. Poix, F. Basile, C. Djega-Mariadassou, Study of parameter cell variation with cation distribution in YFe_3O_4, (1-y) $FeCr_2O_4$ and YFe_3O_4, (1-y) Fe_2SnO_4 system using invariants method, Ann. Chim. 10 (1975) 159–162.

[55] R.D. Shannon, Revised effective ionic radii and systematic studies of interatomic distances in halides and chalcogenides, Acta Crystallogr. 32 (1976) 751–767.

[56] E.J.W. Verwey, Electronic conduction of magnetite (Fe_3O_4) and its transition point at low temperatures, Nature 144 (1939) 327–328.

[57] M.S. Lee, J.U. Meyer, A new process for fabricating CO_2-sensing layers based on $BaTiO_3$ and additives, Sens. Actuators B: Chem. 68 (2000) 293–299.

[58] G. Marsal, A. Dezanneau, J.R. Cornet, Morante, A new CO_2 gas sensing material, Sens. Actuators B: Chem. 95 (2003) 266–270.

[59] D.Y. Kim, H. Kang, N.J. Choi, K.H. Park, H.K. Lee, H.-K, A carbon dioxide gas sensor based on cobalt oxide containing barium carbonate, Sens. Actuators B: Chem. 248 (2017) 987–992.

[60] U. Hoefer, G. Kuhner, W. Schweizer, G. Sulz, K. Steiner, CO and CO_2 thin-film SnO_2 gas sensor on Si substrates, Sens. Actuators B: Chem. 22 (1994) 115–119.